

Gold nanotube encapsulation enhanced magnetic properties of transition metal monoatomic chains: An *ab initio* study

Liyan Zhu,¹ Jinlan Wang,^{1,a)} and Feng Ding²

¹Department of Physics, Southeast University, Nanjing 211189, China

²Institute of Textiles and Clothing, Hong Kong Polytechnic University, Kowloon, Hong Kong

(Received 2 September 2008; accepted 25 November 2008; published online 13 February 2009)

The magnetic properties of gold nanotubes encapsulated transition metal (TM, TM=Co and Mn) and monoatomic chains (TM@Au) are studied using first-principles density functional calculations. The TM chains are significantly stabilized by the gold nanotube coating. TM-TM distance-dependent ferromagnetic-antiferromagnetic phase transition in TM@Au is observed and can be understood by Ruderman-Kittel-Kasuya-Yosida (RKKY) model. The magnetocrystalline anisotropy energies of the TM@Au tubes are dramatically enhanced by one order of magnitude compared to those of free TM chains. Furthermore, the stronger interaction between Mn chain and gold nanotube even switches the easy magnetization axis along the tube. © 2009 American Institute of Physics. [DOI: [10.1063/1.3055520](https://doi.org/10.1063/1.3055520)]

The miniaturization of electronic devices is essential to fabricate high speed and low power electronic circuits.^{1,2} Motivated by this goal, low-dimensional nanoscale structures have been studied intensively for a few decades.³ The one-dimensional (1D) transition metal (TM) monoatomic chain (MAC), whose magnetic properties are much different from those of bulk solid because of significant reduction in dimensionality from three dimensional to real 1D, attracts extensive attention recently.^{4–7} For example, MACs of Sc, Ti, Fe, Co, and Ni are ferromagnetic (FM);^{4,5} whereas the V, Cr, and Mn chains are antiferromagnetic (AFM).^{4,5} Spin polarization of Sc, V, Mn, Fe, Co, and Ni MACs is around 90% or above.⁴ The giant magnetic anisotropy energies of Ni, Tc, Ru, Rh, and Pd MACs suggest that they are promising candidates for ultrahigh density magnetic storages.^{4,6}

It is known that all these freestanding MACs are naturally metastable⁴ and are hard to be used directly in application. So stabilizing these MACs without significantly changing their unique magnetic properties is a critical step toward application. One solution is to encapsulate them into a stable tubular structure.^{8–15} Carbon nanotubes (CNTs) or boron nitrogen nanotubes (BNNTs) have been proposed as good candidates of capsules because of their high stability.^{8,11–14} Whereas recent density functional theory (DFT) study on Fe 5d (Os, Ir, and Pt) nanowires encapsulated in CNTs has indicated that the magnetocrystalline anisotropy energies (MAEs) of the hybrid structures are reduced markedly.¹⁶ Furthermore, the MACs are generally bonded weakly in CNT/BNNT or even endothermic in the formation of the hybrid structures.^{8,9,13}

Gold nanotubes, which have been theoretically proven stable and synthesized experimentally,^{17,18} might be another type of candidate to encapsulate MACs. Recent DFT investigation has revealed that the Fe nanowires encapsulated in Au (6,0) nanotube have large spin polarization at Fermi level

and greatly enhanced MAE.¹⁵ Different from CNT and BNNT, although gold nanotubes are very stable, they are chemically active¹⁹ and thus can interact strongly with the guest atoms. The strong tube-TM interaction is expected to modulate the electronic structures of the guest atoms to enhance their magnetic properties. Motivated by possible enhanced magnetic properties upon encapsulation, our study focuses on the Co and Mn MACs encapsulated in (5,5) gold nanotube (denoted as TM@Au, TM=Co or Mn). To address the advantages of the encapsulated MACs, freestanding TM MACs are also investigated for comparison. Similar to CNT, conceptually, gold nanotube can be made by rolling up a sheet of gold triangular lattice. The notation (n,m) denotes the chiral vector $C=n\mathbf{a}_1+m\mathbf{a}_2$ where \mathbf{a}_1 and \mathbf{a}_2 are the basis vectors of a two-dimensional gold triangular lattice.²⁰ The gold nanotube with indices (5, 5), which has enough hollow to accommodate a MAC inside, has been predicted as the most stable tube theoretically.²⁰ The reason for choosing Co and Mn chains is based on the following considerations. Freestanding Co and Mn MACs are quite different in their magnetic nature, of which ground states are FM and AFM, respectively.^{4,5,21} The magnetic order of Co MAC retains FM configuration in a long interatomic distance range.²¹ In contrast, Mn MACs' magnetic order changes from AFM to FM with increasing interatomic distance.²¹ In addition, when deposited on the (110) surface of Cu, Pd, NiAl, and Ag, the ground state of Mn MACs is AFM, whereas the Co MAC on NiAl (110) surface has almost degenerated FM and AFM solutions (slightly favor FM).²¹ But, when it is deposited on Cu (110) surface, Co MAC favors the FM state.²¹ Briefly, depending on the substrate, the deposited Co and Mn MACs show different distance-magnetism correlations. More precisely, Co MACs always favor FM states whereas the ground state of freestanding Mn MACs changes from AFM to FM with increasing interatomic distance but keeps AFM states if they are deposited on a substrate. On the experimental side Co MACs were successfully deposited on Pt surface and the

^{a)}Electronic mail: jlwang@seu.edu.cn.

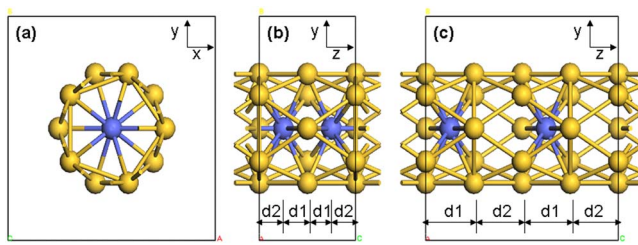


FIG. 1. (Color online) Top view (a) and side view of TM@Au_1 (b) and TM@Au_2 (c). The spheres represent TM and Au atoms.

striking enhanced MAE was observed by Gambardella *et al.*²² Moreover, the oscillatory FM-AFM transition with respect to Co–Co distance was predicted in Co ad-atoms on Cu substrate.²³ Thus we expect that Co and Mn MACs would exhibit new magnetic properties upon gold nanotube coating such as the increased MAE and FM-AFM phase transition with TM interatomic distances.

All the results presented in this work were calculated within the framework of plane-wave DFT implemented in Vienna *ab initio* simulation package (VASP).^{24,25} The exchange-correlation potentials were treated by spin-polarized generalized gradient approximation with PBE (Ref. 26) functional. The interaction between valence electrons and ion cores was described by projected augmented wave^{27,28} method. The conjugate gradient algorithm was used to relax structures until the force acting on each atom was less than 0.01 eV/Å. An energy cutoff, 380 eV, based on convergence tests on total energies of TM@Au systems, was adopted with Methfessel–Paxton²⁹ smearing method to improve self-consistent field (SCF) convergence.

The TM@Au was placed in a supercell with the dimension of $20 \times 20 \times C$ Å³ where C is the lattice constant of supercell alone z (along the axis of Au tube or TM chain) direction. We also considered the low symmetric configurations, in which the Co or Mn atoms are initially placed away

from the central axis of Au tube; however, such configurations are less stable; and all TM atoms optimized back to central axis of the tube. The Au tube between the adjacent periodic images is at least 15 Å, which should be large enough to ignore the interaction between the nearest neighboring tubes. Two different configurations (denoted as TM@Au_1 and TM@Au_2, separately, shown in Fig. 1) are studied in order to investigate the TM–TM distance-dependent magnetic behavior. Each unit cell of the TM chain contains two TM atoms to examine both FM and AFM solutions. The Brillouin zone was meshed by gamma-centered Monkhorst–Pack³⁰ method with $1 \times 1 \times 25$ and $1 \times 1 \times 15$ grids for TM@Au_1 and TM@Au_2, respectively. For spin-orbital coupling, we used denser k-points, $1 \times 1 \times 41$ and $1 \times 1 \times 21$ for TM@Au_1 and TM@Au_2, respectively and the MAE was computed as the full self-consistent total energy difference of the two possible magnetization orientations (parallel and perpendicular to the chain).

The optimized unit length and radius of pure Au (5, 5) tube are 4.57 and 2.48 Å, respectively, which are in good agreement with previous calculations (4.63 and 2.44 Å).²⁰ The calculated Co–Co distances and the FM and AFM Mn–Mn distances in freestanding MAC are 2.16, 2.62, and 2.37 Å, consistent with earlier values of 2.15⁴, 2.60, and 2.29 Å⁵, respectively. For a TM MAC encapsulated in a tube, the TM–TM distance is mainly determined by the lattice parameter of gold nanotube due to the strong tube-TM chain interaction. As seen from Table I, the lattice constant of Co@Au_1 is slightly shorter than that of Mn@Au_1; in TM@Au_2, the discrepancy in the lattice constant is negligible and independent of spin ordering. Thus, the Co–Co distance is also a little shorter than that of Mn–Mn in TM@Au_1 and they are comparable in TM@Au_2. This is because increasing TM–TM distance weakens the TM–TM interaction in TM@Au_2, and as a consequence the encapsulation has less influence on the lattice constant and Co–Co

TABLE I. Equilibrium geometry of freestanding TM wires and TM@Au tubes: MP, lattice constant C (in Å), interatomic distance of TM atoms TM–TM (in Å), and energy difference between AFM and FM $\Delta E_{\text{AFM-FM}}$ (in eV).

System	MP	C	TM–TM	$d1$	$d2$	$\Delta E_{\text{AFM-FM}}$
Co chain	FM	4.31	2.155	0.74
	AFM	4.31	2.155	
Mn chain	FM	5.24	2.620	-0.13
	AFM	4.74	2.370	
Co@Au_1	FM	4.75	2.25/2.50	1.125	1.250	0.48
	AFM	4.79	2.395	1.198	1.198	
Co@Au_2	FM	9.33	4.665	2.348	2.317	-0.08
	AFM	9.33	4.665	2.347	2.318	
Mn@Au_1	FM	4.91	2.455	1.213	1.213	-0.24
	AFM	4.85	2.425	1.228	1.228	
Mn@Au_2	FM	9.28	4.640	2.338	2.302	0.05
	AFM	9.28	4.640	2.338	2.302	

TABLE II. MGS, BE (in eV), total and local spin moments on TM and Au without and with SOC when the magnetization along easy magnetization axis M_S , M_{TMS} , and M_{AuS} , orbital moments M_O , M_{TMO} , and M_{AuO} (in μ_B), and MAE (in meV) of TM chains and TM@Au tubes.

System	MGS	BE	Without SOC			With SOC						
			M_S	M_{TMS}	M_{AuS}	M_S	M_{TMS}	M_{AuS}	M_O	M_{TMO}	M_{AuO}	MAE
Co chain	FM	4.15	4.32	2.10	...	4.39	2.12	...	0.32	0.16	...	-0.88
Mn chain	AFM	2.03	0	± 3.74	...	0	± 3.74	...	0	± 0.04	...	-0.85
Co@Au_1	FM	8.92	4.16	1.90	0.02	4.14	1.89/1.91	0.02	0.20	0.07	0.01	-5.9
Co@Au_2	AFM	9.15	0	± 2.14	± 0.03	0	± 2.10	± 0.03	0	± 0.05	0	-7.08
Mn@Au_1	AFM	7.83	0	± 3.63	0	0	± 3.60	0	0	0.07	0	1.79
Mn@Au_2	FM	9.45	9.62	4.15	0.03	9.62	4.12	0.03	0.05	-0.08	0.01	9.41

distance. Interestingly, the Co MAC in Co@Au_1 is dimerized, but the TM–TM distance is uniform in the rest three encapsulated MACs. This difference can be understood by the strong Co–Co interaction and the longer Co–Co distance in tube than that in a free MAC.

We compute the binding energy (BE) of TM MACs and TM@Au, defined as

$$\text{BE(TM chain)} = 2E(\text{TM}) - E(\text{TM chain}), \quad (1)$$

$$\text{BE(TM @ Au)} = 2E(\text{TM}) + E(\text{tube}) - E(\text{TM @ Au}), \quad (2)$$

separately, where $E(\cdot)$ is the energy of a single TM atom, optimized TM MAC, Au nanotube, and TM@Au. As shown in Table II, the BEs of the TM@Au hybrid structures are remarkably higher than those of free TM MACs, indicating these hybrid structures are very stable. In particular, these BEs are much larger than those of TM@CNT and TM@BNNT, which are usually less than 1 eV per TM atom and some are even endothermic in the formation of hybrid structures [e.g., Fe@CNT(9,0) and Co@BN(9,0)].^{8,9,13} The large BE might stem from the strong hybridization between Au and TM atoms which will be discussed below. Moreover, if we define interaction energy (IE) as the energy differences between TM@Au and the sum of fully optimized gold nanotube and TM MACs, ($\text{IE}(\text{TM @ Au}) = E(\text{TM MAC}) + E(\text{Au tube}) - E(\text{TM @ Au})$), the IEs for Co@Au_1, Co@Au_2, Mn@Au_1, and Mn@Au_2 are 4.77, 5.00, 5.80, and 7.42 eV, respectively. This implies that the TM MACs are significantly stabilized and the tube-MAC interaction is as strong as the TM–TM interaction. Therefore, TM@Au tubes are very stable against disintegrating into their constituents; and thus it is possible to synthesize these hybrid structures experimentally.

The FM state of Co@Au_1 is 0.48 eV lower in energy than the AFM state and has a total magnetic moment of $4.16\mu_B$ per unit cell. In the FM state, the spins on a Au atom ($\sim 0.02\mu_B$) is negligible compared to that on a Co atom ($1.90\mu_B$). However, the AFM state of Co@Au_2 is 0.08 eV lower in energy than the FM state, showing a magnetic phase (MP) transition from FM to AFM. In contrast, the AFM state of Mn@Au_1 is more stable than the FM one with an energy difference of 0.24 eV per unit cell. The two Mn atoms in the AFM state have opposite spins of $3.63\mu_B$ on each one. The

FM state of Mn@Au_2 is the ground state and has a giant magnetic moment ($9.62\mu_B$ per unit cell). Inverse to that in Co@Au, MP transitions from the AFM state to the FM state are identified in Mn@Au. Density of states (DOS) analysis results show that the TM–TM interaction plays a dominant role in TM@Au_1 and the TM–TM interaction is negligible in TM@Au_2 due to the elongated TM–TM distance (see Figs. 2 and 3). As a consequence, the ground magnetic ordering of TM@Au_2 is dominated by the indirect exchange interactions, which the TM atoms interact through the intermediate of the hybridization of Au s electrons and TM d electrons (also see Fig. 2). This is a typical Ruderman–Kittel–Kasuya–Yosida (RKKY) type exchange interaction, which is characterized with a damped oscillation over a relatively long atom–atom distance range, and transition from FM/AFM to AFM/FM may happen.^{31,32} The negative (positive) exchange integral of Co@Au_2 (Mn@Au_2) will thus give rise to the AFM (FM) ground states. Calculating the RKKY exchange integral quantitatively is beyond this study. Therefore, the transitions from FM to AFM in Co@Au and from AFM to FM in Mn@Au take place when the TM–TM distances increase.

The spin orbit coupling (SOC) is taken into account as well to examine the magnetocrystalline anisotropy. The MAE is defined as the energy difference between the magnetizations oriented along x and z directions, namely, $\text{MAE} = E(x) - E(z)$, where z is the tube axis direction. The MAEs for both freestanding Co and Mn MACs are negative, indicating that the magnetization prefers to be perpendicular to the chain axis, which is in agreement with the previous theoretical result.⁴ When encapsulated in a Au tube, the MAEs are all remarkably enhanced by one order of magnitude and a trend that longer TM–TM distance results in a larger MAE is observed. In application of ultrahigh density information storage, the notably enhanced MAE is important to overcome the disorder resulted from thermal fluctuation. Besides, in contrast to Co@Au, the easy magnetization axes of the Mn@Au switch from that perpendicular to the axes in the free Mn MAC to that along the axes. The possible reasons for the change in easy magnetization directions in Mn@Au might stem from the stronger interaction between Mn wires and Au tubes as discussed above (5.80 versus 4.77 eV for TM@Au_1, and 7.42 versus 5.0 eV for TM@Au_2 for Co and Mn, respectively). The easy magnetization direction

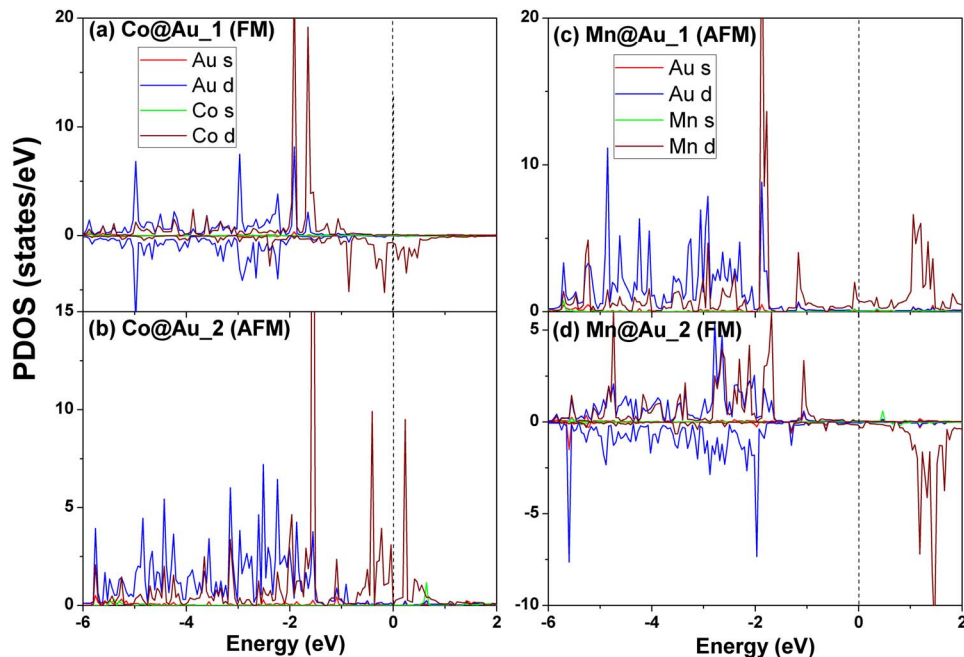


FIG. 2. (Color online) Atom resolved partial DOS of Co@Au_1 (a), Co@Au_2 (b), Mn@Au_1 (c), and Mn@Au_2 (d). The dotted line refers to the Fermi level.

along the tube axes in Mn@Au makes them possible for practical application.¹⁶

Figures 2 and 3 present the spin-polarized partial density of states (PDOS) and charge density of Co@Au_1, Co@Au_2, Mn@Au_1, and Mn@Au_2 in the magnetic ground states (MGSSs), respectively. The states of Au atoms strongly hybrid with those of TM atoms between -6 and -2 eV; while around Fermi level the states are mainly contributed by TM atoms. One can see that the TM *d* states strongly interact with Au *d* states but minor Au *s*-TM *d* states overlapping indicating the weak *s-d* hybridizations (Fig. 2). The strong hybridization of TM *d* states and Au *d* states are responsible for the high stability of TM@Au tube. The *s* electrons of Au atoms are the intermediate of the

RKKY exchange interaction between TM atoms. The *d* states can be divided into three groups: nondegenerate d_z^2 states, double degenerate ($d_{x^2-y^2}, d_{xy}$) states, and (d_{xz}, d_{yz}) states. The double degenerate ($d_{x^2-y^2}, d_{xy}$) and (d_{xz}, d_{yz}) states of TM bond with those of Au, while the d_z^2 states of the TM atom form strong σ bonds.

The bond features can also be intuitively demonstrated by the charge density distribution. As shown in Fig. 3, the charge distributed between the nearest neighboring Co pair is denser than that between the second nearest neighbors in Co@Au_1 [Fig. 3(a)]. Therefore, the dimerization, probably due to Peierls instability,³³ in Co@Au_1 occurs. For TM@Au_2, the larger TM-TM distances diminish the orbital overlap between neighboring TM atoms and thus the σ bond (d_z^2) between TM atoms breaks. This also can be seen from the charge density distribution as shown in Figs. 3(b) and 3(d). The TM atoms, as a result, only bond with the nearest ten Au atoms. Therefore, the d_z^2 states become much sharper than in TM@Au_1 [see Fig. 2], which eventually leads to greatly enhanced electron localization in TM@Au_2.

To summarize, we have carried out spin-polarized *ab initio* computations to study the hybrid structures of the Co and Mn MACs encapsulated in gold nanotubes. The strong *d-d* hybridization of TM@Au significantly stabilizes the TM MACs. Increasing Co-Co distances in Co@Au nanotube results in a transition from FM to AFM, whereas Mn@Au nanotubes exhibit a totally opposite transition from AFM to FM. Moreover, the MAEs of encapsulated MACs are one order of magnitude larger than those of free MACs owing to the increased TM-TM distances. The larger MAE suggests that the hybrid structures can be used in ultrahigh density magnetic storage. Because of the stronger interactions between Mn wires and Au tubes, the easy magnetization directions of Mn@Au change from that perpendicular to the axes in the free Mn MAC to that along the axes.

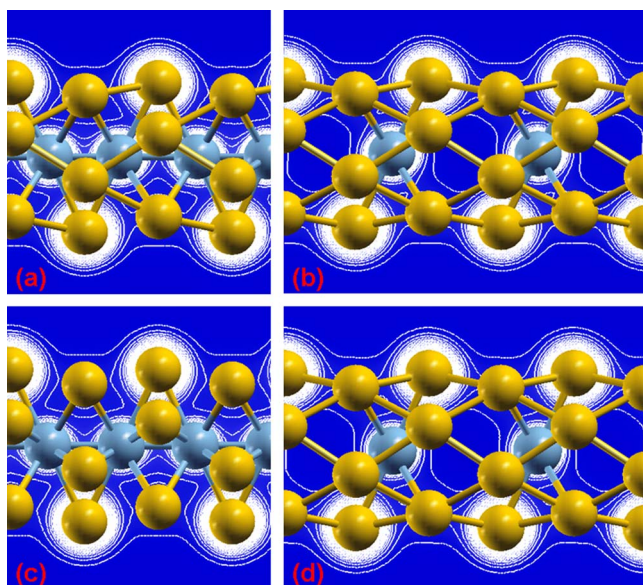


FIG. 3. (Color online) Contours of charge density on a plane parallel xz and passing TM atoms of Co@Au_1 (a), Co@Au_2 (b), Mn@Au_1 (c), and Mn@Au_2 (d).

The work is supported by the NSF of China (Grant Nos. 10604013 and 20873019), the Program for New Century Excellent Talents in the University of China (Grant No. NCET-06-0470), the project sponsored by SRF for ROCS, SEM, the Qinglan Project in Jiangsu Province, and the Outstanding Young Faculty and Peiyu funding of Southeast University. The authors would like to thank the computational resource at Department of Physics, Southeast University.

- ¹Y. Huang, X. Duan, Y. Cui, L. J. Lauhon, K. H. Kim, and C. M. Lieber, *Science* **294**, 1313 (2001).
- ²G. Y. Tseng and J. C. Ellenbogen, *Science* **294**, 1293 (2001).
- ³F. J. Himpsel, J. E. Ortega, and G. J. Manke, *Adv. Phys.* **47**, 511 (1998).
- ⁴J. C. Tung and G. Y. Guo, *Phys. Rev. B* **76**, 094413 (2007).
- ⁵C. Ataca, S. Cahangirov, E. Durgun, Y. R. Jang, and S. Ciraci, *Phys. Rev. B* **77**, 214413 (2008).
- ⁶Y. Mokrousov, G. Bihlmayer, S. Heinze, and S. Blugel, *Phys. Rev. Lett.* **96**, 147201 (2006).
- ⁷A. Delin and E. Tosatti, *Phys. Rev. B* **68**, 144434 (2003).
- ⁸C. K. Yang, J. Zhao, and J. P. Lu, *Phys. Rev. Lett.* **90**, 257203 (2003); *Phys. Rev. B* **74**, 235445 (2006).
- ⁹M. Weissmann, G. García, M. Kiwi, R. Ramírez, and C. C. Fu, *Phys. Rev. B* **73**, 125435 (2006).
- ¹⁰H. Shiroishi, T. Oda, H. Sakashita, and N. Fujima, *Eur. Phys. J. D* **43**, 129 (2007).
- ¹¹L. Liu, S. Mu, S. Xie, W. Zhou, L. Song, D. Liu, S. Luo, Y. Xiang, Z. Zhang, X. Zhao, W. Mal, J. Shen, C. Wang, and G. Wang, *J. Phys. D* **39**, 3939 (2006).
- ¹²L. Guan, K. Suenaga, S. Okubo, T. Okazaki, and S. Iijima, *J. Am. Chem. Soc.* **130**, 2162 (2008).
- ¹³H. J. Xiang, J. Yang, J. G. Hou, and Q. Zhu, *New J. Phys.* **7**, 39 (2005).
- ¹⁴D. Golberg, F. F. Xu, and Y. Bando, *Appl. Phys. A: Mater. Sci. Process.* **76**, 479 (2003).
- ¹⁵Y. Mokrousov, G. Bihlmayer, and S. Blügel, *Phys. Rev. B* **72**, 045402 (2005).
- ¹⁶J. Wang, C. Jo, and R. Wu, *Appl. Phys. Lett.* **92**, 032507 (2008).
- ¹⁷M. Wirtz and C. R. Martin, *Adv. Mater. (Weinheim, Ger.)* **15**, 455 (2003).
- ¹⁸Y. Oshima and A. Onga, *Phys. Rev. Lett.* **91**, 205503 (2003).
- ¹⁹W. An, Y. Pei, and X. C. Zeng, *Nano Lett.* **8**, 195 (2008).
- ²⁰R. T. Senger, S. Dag, and S. Ciraci, *Phys. Rev. Lett.* **93**, 196807 (2004).
- ²¹Y. Mokrousov, G. Bihlmayer, S. Blügel, and S. Heinze, *Phys. Rev. B* **75**, 104413 (2007).
- ²²P. Gambardella, A. Dallmeyer, K. Maiti, M. C. Malagoli, W. Eberhardt, K. Kern, and C. Carbone, *Nature (London)* **416**, 301 (2002).
- ²³P. Wahl, P. Simon, L. Diekhöner, V. S. Stepanyuk, P. Bruno, M. A. Schneider, and K. Kern, *Phys. Rev. Lett.* **98**, 056601 (2007).
- ²⁴G. Kresse and J. Hafner, *Phys. Rev. B* **48**, 13115 (1993).
- ²⁵G. Kresse and J. Furthmüller, *Comput. Mater. Sci.* **6**, 15 (1996).
- ²⁶J. P. Perdew, K. Burke, and K. Ernzerhof, *Phys. Rev. Lett.* **77**, 3865 (1996).
- ²⁷P. E. Blochl, *Phys. Rev. B* **50**, 17953 (1994).
- ²⁸G. Kresse and D. Joubert, *Phys. Rev. B* **59**, 1758 (1999).
- ²⁹M. Methfessel and A. T. Paxton, *Phys. Rev. B* **40**, 3616 (1989).
- ³⁰H. J. Monkhorst and J. D. Pack, *Phys. Rev. B* **13**, 5188 (1976).
- ³¹M. A. Ruderman and C. Kittel, *Phys. Rev.* **96**, 99 (1954).
- ³²K. Yosida, *Phys. Rev.* **106**, 893 (1957).
- ³³R. E. Peierls, *Quantum Theory of Solids* (Clarendon, Oxford, 1955), p. 108.